The Journal of Experimental Biology 210, 1868-1873
Published by The Company of Biologists 2007
doi:10.1242/jeb.003772

Morphological diversity of medusan lineages constrained by animal–fluid interactions

John O. Dabiri[1,*], Sean P. Colin[2] and John H. Costello[3]

[1]*Graduate Aeronautical Laboratories and Bioengineering, California Institute of Technology, Pasadena, CA 91125, USA,* [2]*Environmental Sciences, Roger Williams University, Bristol, RI 02809, USA and* [3]*Biology, Providence College, Providence, RI 02918, USA*

*Author for correspondence (e-mail: jodabiri@caltech.edu)

Accepted 11 March 2007

Summary

Cnidarian medusae, commonly known as jellyfish, represent the earliest known animal taxa to achieve locomotion using muscle power. Propulsion by medusae requires the force of bell contraction to generate forward thrust. However, thrust production is limited in medusae by the primitive structure of their epitheliomuscular cells. This paper demonstrates that constraints in available locomotor muscular force result in a trade-off between high-thrust swimming *via* jet propulsion and high-efficiency swimming *via* a combined jet-paddling propulsion. This trade-off is reflected in the morphological diversity of medusae, which exhibit a range of fineness ratios (i.e. the ratio between bell height and diameter) and small body size in the high-thrust regime, and low fineness ratios and large body size in the high-efficiency regime. A quantitative model of the animal–fluid interactions that dictate this trade-off is developed and validated by comparison with morphological data collected from 660 extant medusan species ranging in size from 300 μm to over 2 m. These results demonstrate a biomechanical basis linking fluid dynamics and the evolution of medusan bell morphology. We believe these to be the organising principles for muscle-driven motility in Cnidaria.

Supplementary material available online at
http://jeb.biologists.org/cgi/content/full/210/11/1868/DC1

Key words: locomotion, biomechanics, fluid dynamics, medusae.

Introduction

The influence of fluid environments on the evolution of body plans of swimming and flying animals has long been a focus of evolutionary and functional biologists (e.g. Thompson, 1961; Vogel, 2003). Central to understanding the importance of evolved morphological features of these animals is the determination of how the animal interacts with the surrounding fluid (i.e. water or air). Jellyfish are the earliest known metazoans to use muscle power for swimming (Valentine, 2004). As cnidarians, they are limited in the morphological structures available for propulsion (Gladfelter, 1972a,b; Chapman, 1974). Nonetheless, they are often identified as highly proficient jet propellers (Donaldson et al., 1980; Mackie, 1980). Jet propulsion is an energetically expensive, but highly effective, mode of propulsion (Daniel, 1985).

Prevailing models of jet propulsion describe the forces that medusae use for swimming to be generated solely during the swimming power stroke. The jet propulsive force is generated by the contraction of the circular muscle fibers lining the surface of the subumbrellar cavity, exerting pressure (force/subumbrellar area) on the fluid in the cavity and forcing it out of the bell. Following bell contraction, a single vortex ring is formed in the wake (termed the ‘starting’ vortex) and the momentum imparted to the fluid during this power stroke provides the force available for forward motion (Fig. 1A; see also Movie 1 in supplementary material) (Dabiri et al., 2006). Therefore, the force available for thrust is directly related to, and even less than (e.g. due to necessary elastic storage and mechanical losses) (DeMont and Gosline, 1988a; DeMont and Gosline, 1988b; DeMont and Gosline, 1988c), the force of the contracting muscle fibers.

The contractile muscle fibers are only one cell layer thick and are a primitive feature that, among the metazoans, is only used by cnidarians for motility (Fawcett, 1994). In addition, they limit the force that medusae can generate for jet propulsion because the muscular contractile forces required to achieve jet propulsion do not scale favorably with increasing medusa size (Bonner, 1965; Valentine, 2004). Specifically, the mass of water expelled from a medusa bell with diameter D scales as D^3, whereas the muscle force required to accelerate that mass only scales as D^1 [i.e. muscle force~muscle cross-sectional area=muscle thickness (a constant)×muscle sheet width (~D) (Gladfelter, 1974; Chapman, 1974)]. Therefore the force required for jet

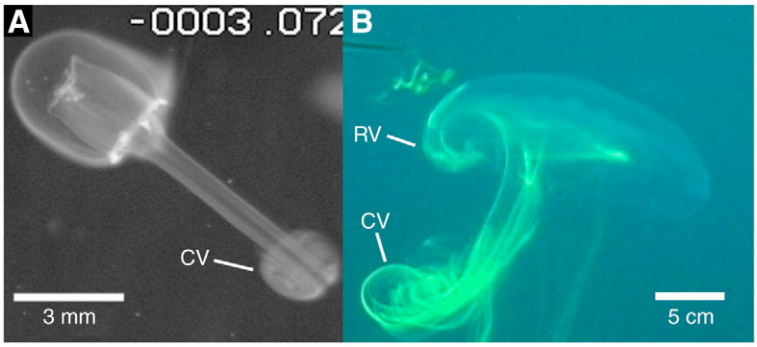

Fig. 1. Visualizations of medusa flow currents. (A) Jet propulsion in juvenile *Aequorea victoria*. A vortex ring (CV) is formed in the water during the bell contraction phase, whereas no vortex is formed in the water during the bell relaxation phase. (B) Jet-paddling in *Aurelia aurita*. Vortex rings of opposing rotational orientation are formed in the water during bell contraction (CV) and relaxation (RV), respectively. The stopping vortex can be observed forming near the bell margin (RV). This vortex will interact with the subsequent contraction phase vortex, affecting swimming thrust and efficiency (see text).

propulsion increases with animal size more rapidly than the available physiological force.

In this paper, we use models that compare the forces produced by medusae to the forces required for propulsion, in order to investigate how fluid interactions may constrain medusan bell morphology across the extant species. The developed analytical models are validated by comparison with *in situ* field and laboratory observations of freely swimming *Aurelia aurita* and juvenile *Aequorea victoria* medusae, respectively. These species have been selected for wake studies because they represent distinct regions of medusan morphospace. In particular, *Aurelia* is typically larger and more oblate (flatter) while juvenile *Aequorea* is smaller and prolate (torpedo-shaped). To complement the studies of wake kinematics, we also examine morphological data collected from measurements of 660 extant species reported in the literature. The following section describes the experimental and analytical methods.

Materials and methods

Visualization of animal-fluid interactions

Specimens of newly budded *Aequorea victoria* (Agassiz 1849), a prolate juvenile hydromedusa native to the Puget Sound, WA, USA, were received from the New England Aquarium, Boston, MA, USA. To visualize their wake during swimming, individuals were placed into a 200 ml rectangular filming vessel filled with saltwater, and video recordings at 250 frames s^{-1} were made following published methods (Costello and Colin, 1994) using a 720×480-pixel CCD camera connected to a PC. The wake flow was made visible by injecting fluorescein dye around the medusa prior to bell contraction.

Measurements of *Aurelia aurita* (Linnaeus 1746), an oblate scyphomedusa, were collected from a marine lake (145 hectares, maximum depth 46 m) on the island of Mljet, Croatia, located in the Adriatic Sea (latitude: 42.75°N, longitude: 17.55°E) during July 2003. All of the video was recorded in shallow water (<20 m) by SCUBA using natural light. Video was recorded at 30 frames s^{-1} on miniDV videotape using a Sony DCR VX2000 camera with a zoom lens contained within an Amphibico underwater housing (Amphibico, Inc., Montreal, QC, Canada). A second diver injected 20 μl pulses of concentrated fluorescein dye into the water at specific locations around the medusae.

Mathematical derivation of morphological diversity models

The proposed morphological diversity model is based on an expression for the net time-averaged locomotive force required for swimming:

$$F_L = (T_J/T)F_J - (T_R/T)F_R \,, \quad (1)$$

where T_J and T_R are the durations of the jetting and relaxation phases, respectively, T is the duration of the entire swimming cycle (i.e. $T=T_J+T_R$), and F_J and F_R are the locomotive forces occurring during the jetting and relaxation phases, respectively. The negative sign before the second term accounts for the direction of the relaxation phase force opposite to the contraction phase force. For clarity in the following analysis, we will henceforth neglect the weighted times T_J/T and T_R/T without a loss of generality in the results.

The force F_J during bell contraction is calculated using the model of Daniel (Daniel, 1983):

$$F_J = (\rho/A)\,(dV/dt)^2 \,, \quad (2)$$

where $A=\pi D^2/4$ is the oral cavity exit area and V is the volume of the oral cavity. Approximating the oral cavity volume as a hemiellipsoid, its volume is related to the bell height H and diameter D as $V=(\pi/6)HD^2$. Hence its time-derivative is:

$$\frac{dV}{dt} = \frac{\pi}{6}\left(2HD\frac{dD}{dt} + \frac{dH}{dt}D^2\right). \quad (3)$$

The time-derivative dV/dt of the oral cavity volume is dependent on changes in the bell diameter dD/dt during the swimming cycle to a much greater degree than changes in the bell height dH/dt, due to both the quadratic dependence of oral cavity volume on bell diameter (compared to linear dependence on bell height) and the physiologically observed greater motion of the bell diameter relative to the bell height during the swimming cycle. Therefore we may approximate Eqn 3 as:

$$\frac{dV}{dt} \approx \frac{\pi}{3} HD\frac{dD}{dt} \,. \quad (4)$$

The force F_R due to bell relaxation can be estimated based on the strength of the 'stopping vortex' that may form due to bell

motion during this phase of the swimming cycle (Dabiri et al., 2005; Dabiri et al., 2006):

$$F_R \approx \rho A_V \Gamma / T_R \ , \quad (5)$$

where A_V is the area enclosed by the vortex ring and Γ is the vortex ring circulation, a measure of its strength. The vortex ring enclosed area A_V can be approximated by the oral cavity area $A=\pi D^2/4$, since the vortex is formed at the bell margin and remains attached to the body until the end of the relaxation phase. The vortex ring circulation can be calculated by applying the slug model (Didden, 1979) to the flow at the bell margin, where the characteristic flow velocity is given by the bell motion dD/dt, i.e. $\Gamma \approx \frac{1}{2}(\frac{1}{2}dD/dt)^2 T_R$.

Combining these results in Eqn 5:

$$F_R \approx \frac{\pi}{32} \rho D^2 \left(\frac{dD}{dt}\right)^2 . \quad (6)$$

By substituting Eqn 2, Eqn 4 and Eqn 6 into the governing force equation, Eqn 1 becomes:

$$F_L \approx \frac{4\pi}{9} \rho \left(H \frac{dD}{dt}\right)^2 - \frac{\pi}{32} \rho \left(D \frac{dD}{dt}\right)^2 . \quad (7)$$

Since the fineness ratio $f=H/D$, the bell height can be eliminated from Eqn 7:

$$F_L \approx \rho \left(\frac{4\pi}{9} f^2 - \frac{\pi}{32}\right) \left(D \frac{dD}{dt}\right)^2 . \quad (8)$$

Solving for the fineness ratio and applying the functional constraint that the maximum locomotive force F_L is bounded by the physiological force F_M that can be applied by the subumbrellar muscle fibers (i.e. $F_L \leqslant F_M$),

$$f \leqslant \sqrt{\frac{9}{4\pi\rho} \left[\frac{\pi\rho}{32} + F_M \left(D \frac{dD}{dt}\right)^{-2} \right]} . \quad (9)$$

The physiological force F_M is the mathematical product of the maximum muscle stress σ_M, subumbrellar muscle sheet thickness τ_M, and muscle sheet width, which has been observed to be roughly one half of the bell diameter D (Gladfelter, 1972):

$$F_M = \sigma_M \tau_M D / 2 . \quad (10)$$

The time-dependent bell diameter motion can be modeled as a trigonometric function that attains the resting bell diameter D at the beginning of the swimming cycle and contracts to $D/2$ at the transition from bell contraction to bell relaxation (Gladfelter, 1972a,b; Ford and Costello, 2000). For simplicity and generality, we currently utilize the function $(D/4)(3+\cos\omega t)$, where ω is the swimming frequency in rad s^{-1} and the swimming cycle occurs over a period of duration T, i.e. $0 \leqslant t \leqslant T = 2\pi/\omega$. Functions that more faithfully represent the bell motion of each species could also be used here. However, we will show that this simple approximation is sufficient to explain the observed trends in the morphological data without appealing to the detailed kinematics of each species. Substituting this function into Eqn 9 gives:

$$f \leqslant \sqrt{\frac{9}{4\pi\rho} \left(\frac{\pi\rho}{32} + \frac{\sigma_M \tau_M}{2g(\omega)D^3} \right)} , \quad (11)$$

where the frequency-dependent function $g(\omega)$ is given by the time average of $[D(dD/dt)]^2$ over the duration of one swimming cycle. For the trigonometric function used presently, $g(\omega)$ is given by:

$$g(\omega) = \frac{\omega}{2\pi} \int_0^{2\pi/\omega} \frac{1}{256} \omega^2 \sin^2\omega t (3+\cos\omega t)^2 dt . \quad (12)$$

Since the fineness ratio $f=H/D$, both sides of Eqn 11 can be multiplied by D to determine an approximate relationship between bell height and diameter across medusan lineages:

$$H \sim \sqrt{D^2 + C/D} , \quad (13)$$

where C is a dimensional constant with units of volume.

Results

We first compare the forces generated by the muscle fibers (F_M) to the forces required for jet-propelled locomotion (F_J), i.e. where stopping vortex formation is neglected in Eqn 1. In order to swim at a given frequency ω, F_M must be greater than or equal to F_J. The parameter F_M is the product of muscle cross-section area and the isometric stress of the muscle tissue; therefore, its magnitude is a function of bell size and shape. Likewise, for jet propulsion, F_J is related to the volume of the subumbrellar cavity, the oral cavity exit area, and their respective changes with bell size and shape (Daniel, 1983). Fig. 2A plots the size-limiting curve $F_M=F_J$ for medusa shape (quantified by the fineness ratio f=bell height H/bell diameter D) *versus* bell diameter D for various swimming frequencies. This curve is generated by plotting Eqn 11 while neglecting the first term in parenthesis, which arose due to the presence of the stopping vortex. These limiting upper-bound curves illustrate that for most bell shapes (i.e. fineness ratios), medusae larger than 10 cm cannot produce a sufficient muscle force to swim *via* jet propulsion.

However, some species of medusae are known to reach diameters greater than 2 m (e.g. Omori and Kitamura, 2004), apparently violating the predicted size limits for jetting medusae. The present field observations of *Aurelia* show that oblate medusae (i.e. low fineness ratios) create more complex wake structures than those of more prolate jetting medusae (i.e. high fineness ratios; Fig. 1A), and swim with a combined jet-paddling mode of propulsion (also termed rowing; Fig. 1B; see also Movie 2 in supplementary material) (Dabiri et al., 2005). In jet-paddling medusae, the contraction phase generates a starting vortex similar to that of traditional jetting medusae. However, during the relaxation phase the paddling motion of the bell causes the formation of a second, stopping vortex ring

with opposite rotational orientation relative to the starting vortex.

Including the effect of the stopping vortex in Eqn 1 and using average physiological and kinematic values (Gladfelter, 1972a; Gladfelter, 1972b; Anderson and Schwab, 1981; Bone and Trueman, 1982) for σ_M (160 kPa), τ_M (3.5 μm) and ω (π, 2π and 4π rad s^{-1}), Fig. 2B plots the predicted morphological distribution of fineness ratio *versus* bell diameter for all medusae swimming at various bell contraction frequencies (i.e. Eqn 11). The new model predicts that the bell diameter for oblate jet-paddling medusae is not constrained by physiological limits, as prolate jetting medusae are. In other words, according to the model, medusae with lower fineness ratios create sufficient stopping vortices during bell relaxation to effectively reduce the forces required for locomotion. Consequently, oblate medusae of any size are able to generate sufficient muscle forces to swim. Interestingly, the model predicts that across all medusan lineages there exists a universal critical fineness ratio f_{CRIT} below which medusae of any bell diameter can exist, $f_{CRIT}=\sqrt{9/128}\approx0.265$.

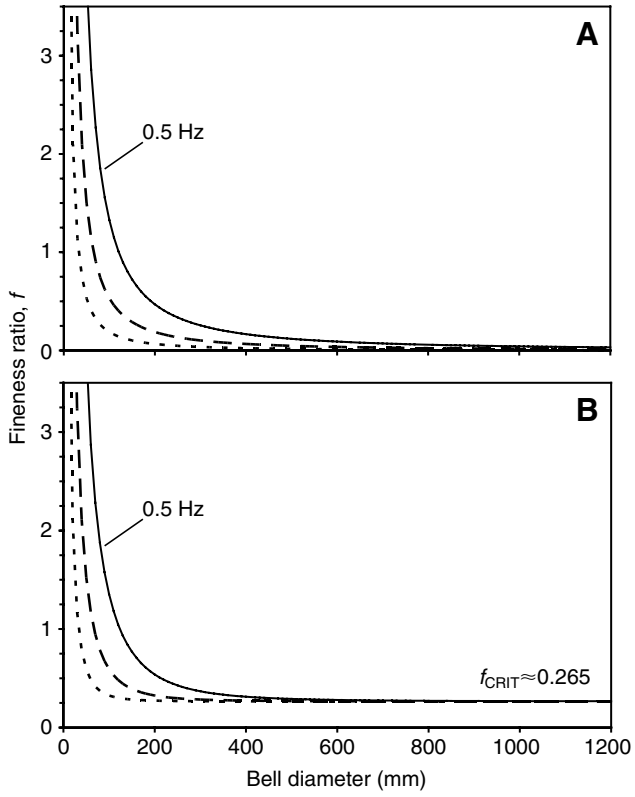

Fig. 2. Quantitative model of force balance between the force F_M produced by medusan muscle contraction and the forces F_J or F_L required for locomotion. Solid line, 0.5 Hz swimming frequency model; broken line, 1 Hz model; dotted line, 2 Hz model. The constraint on morphological diversity becomes more severe with increasing swimming frequency due to the increased flow accelerations and required locomotive forces. (A) Limiting curve corresponding to force balance $F_M=F_J$, i.e. Eqn 11 plotted with the first term in parenthesis neglected. The model predicts that jet-propelled medusae are limited to the morphospace below this curve, i.e. medusae with bell shape and size combinations above the curve are not capable of swimming *via* jet propulsion. (B) Limiting curve corresponding to force balance $F_M=F_L$, i.e. Eqn 11. The new model predicts that all medusae are limited to the morphospace below this curve. At high fineness ratios the force constraints for jet-paddling and jet propulsion do not differ significantly because magnitude of the stopping vortex during the recovery stroke of jet-paddling is inversely related to fineness ratio. At low fineness ratios the stopping vortex sufficiently reduces F_L such that it is never greater than F_M; therefore, medusan sizes are not constrained below the critical fineness ratio $f_{CRIT}=\sqrt{9/128}\approx0.265$. This is the key difference between A and B.

If these medusae–fluid interactions are influential in constraining the evolution of bell morphology we would expect to observe a similar relationship between bell diameter and fineness ratio for most extant medusan species. A medusan morphospace, compiled from average bell diameter and height values of all of the medusae published or illustrated in monographs describing hydromedusae (Kramp, 1959; Kramp, 1961; Kramp, 1968), scyphomedusae (Mayer, 1910), or siphonophores (Pugh, 1999), reveals that the relationship between bell fineness and diameter is not random and that bell shape is highly dependent on bell size (Fig. 3; see Table S1 in supplementary material). At small bell diameters (<50 mm), bell shape is highly variable between oblate and prolate forms. However, at larger bell diameters (>200 mm), only oblate bell forms exist in nature. As a result, there is a large region of potential bell size and shape combinations unoccupied by any medusa.

Fig. 4A plots the predicted morphological distribution of fineness ratio *versus* bell diameter for various swimming frequencies and compares these predictions with the morphological data. The model accurately predicts the observed bounds on the morphological distribution of medusae, especially those exhibiting the largest bell diameters where the critical fineness ratio f_{CRIT} is approached. If the formation of

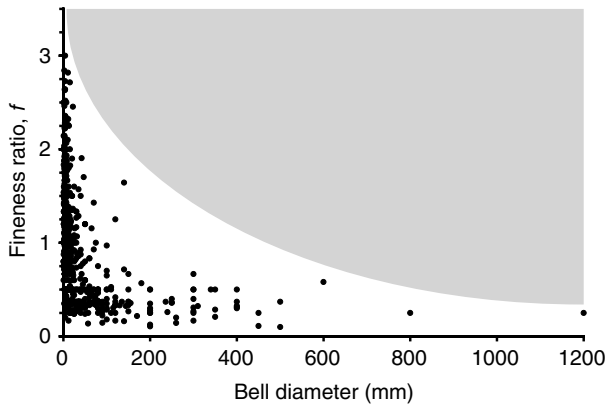

Fig. 3. Medusan morphospace (fineness ratio, *f*, *versus* bell diameter, *D*) derived from morphological data of 660 extant species of medusae. The figure illustrates a non-random relationship between bell shape and size. The shaded area identifies shape and size combinations that do not exist among extant medusae.

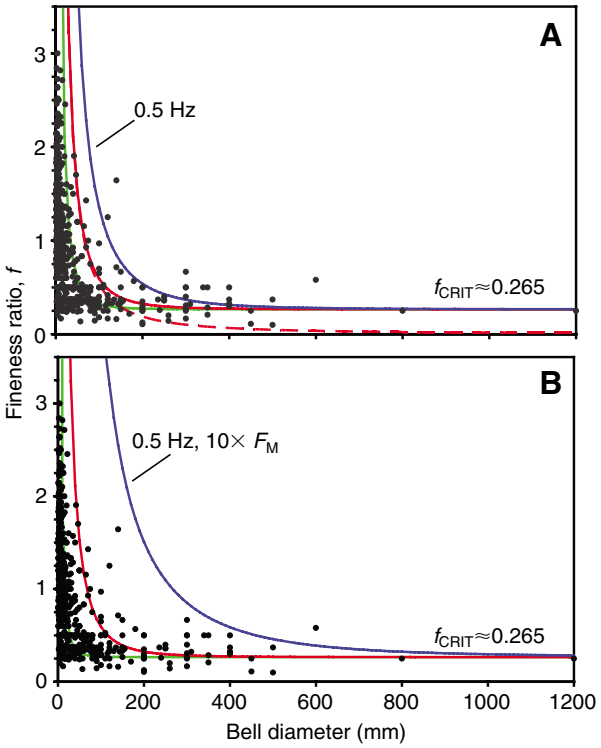

Fig. 4. Comparison of quantitative model of morphological diversity with data from 660 extant species of medusae. (A) Black circles, morphological data; solid blue curve, 0.5 Hz swimming frequency model; solid red curve, 1 Hz model; solid green curve, 2 Hz model. Broken red curve, model prediction in the absence of stopping vortex formation at 1 Hz. (B) Black circles, morphological data; solid blue curve, morphospace limit corresponding to an order of magnitude increase (10 times) in the physiologically available force F_M for the model with 0.5 Hz swimming frequency; solid green curve, morphospace limit corresponding to an order of magnitude decrease (0.1 times) in the physiologically available force F_M for the model with 2 Hz swimming frequency; red curve, 1 Hz model corresponding to average physiological data. f_{CRIT}, critical fitness ratio.

the stopping vortex is neglected in the model, as in the traditional jet propulsion perspective, Fig. 4A also shows that the largest medusae would appear to violate the constraint imposed by the available muscle capacity. The sensitivity of these results to the muscle capacity estimate is explored in the following Discussion section.

Finally, plotted on a log–log scale with H on the ordinate axis and D^2+C/D on the abscissa, the model (i.e. Eqn 13) predicts that the morphological data for bell height *versus* diameter should lie on a line with slope=1/2, i.e. $\log H \sim \frac{1}{2}\log(D^2+C/D)$. Fig. 5 compares this model with the morphological data. The agreement is reasonable, although a least-squares fit to the data suggests a smaller slope of 0.37. Most of the discrepancy occurs at large bell diameters, where the model assumption that $dH/dt \ll dD/dt$ becomes less accurate (see Materials and methods). A curvilinear model could be incorporated to account for the slope change at large bell diameters. However, this would necessitate either an arbitrary curve-fitting constant or the

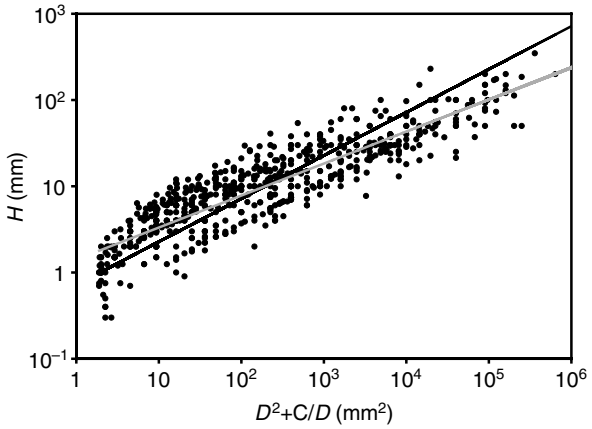

Fig. 5. Relationship between bell height H and the function of bell diameter D derived in Eqn 13 for 660 extant species of medusae. Black circles, morphological data; black line, model prediction with slope=0.5; grey line, least-squares fit with slope=0.37.

future discovery of additional scaling constraints that can be combined with the present analysis.

Discussion

The presence of the stopping vortex ring has implications not only for swimming force, which is the primary focus of this paper, but also for hydrodynamic efficiency. In the process of generating the forces necessary for locomotion, kinetic energy is inevitably lost to the wake. The magnitude of this kinetic energy loss, related to the induced drag (Lighthill, 1960), is directly proportional to the amount of rotational motion in the medusa wake. The stopping vortex interacts with the contraction-phase starting vortex of the next swimming cycle through mutual cancellation of their opposite-signed vorticity and through the velocity fields that they induce upon one another (i.e. Biot–Savart induction) (Saffman, 1992). These interactions reduce the total rotational motion in the water behind the animal (Fig. 1B; see also Movie 2 in supplementary material and Figs 2 and 3) (Dabiri et al., 2005). Hence, motion-canceling between the starting and stopping vortices in the jet-paddling swimming mode acts to reduce the kinetic energy lost in the wake, thereby increasing the swimming efficiency. This is in contrast with conventional jet-propulsion, which suffers from reduced hydrodynamic efficiency due to the large quantity of kinetic energy that is deposited into the wake during thrust production (Vogel, 2003) (cf. Fig. 1A). Interestingly, a similar energy-recovery mechanism has been identified in the swimming of bony fishes (Ahlborn et al., 1991; Ahlborn et al., 1997). However, the existence of such energy-saving behaviors has not previously been appreciated in lineages as primitive as medusae.

The developed model is especially useful because of the small number of input parameters required to make predictions. Nonetheless, it relies on a quasi-steady approximation of transient swimming dynamics and muscle

mechanics. There may potentially exist variations in muscle performance across medusan lineages due to differences in muscle myosin isoforms, twitch durations, shortening velocities, sarcomere geometries, etc. Models explicitly incorporating these effects have been shown to require a large number of input parameters (Daniel, 1995), which detracts from the goals of the present model. However, Fig. 4B shows that even if the combined effect of these variations were to change the nominal physiologically available force computed above by an order of magnitude (i.e. $0.1F_M$ or $10F_M$), the predicted morphological distribution would be relatively unaffected. Mathematically, this robustness of the model follows from the relatively weak (i.e. square-root) dependence of the limiting curves on the physiological force (cf. Eqn 11). To be sure, an order of magnitude variation in the physiological force F_M is highly unlikely, given that cnidarians are limited to a single cell layer of muscle. We hypothesize that the outliers in the data exhibit departures from the assumed bell kinematics rather than the bell mechanics. However, the present data are insufficient to resolve this question conclusively.

In conclusion, the present model and the supporting morphological data indicate that animal–fluid interactions provide organising principles for the most primitive form of muscle-powered locomotion. The physiological limits of medusan force generation have determined the permissible range of medusan design solutions to swimming in a fluid environment, and in general, two solutions have emerged: medusae may be either small and jet-propelled or oblate and propelled by jet-paddling.

The authors acknowledge support from the NSF Ocean Sciences Division – Biological Oceanography Program (OCE-0623475 awarded to J.O.D., OCE-0351398 and -0623534 awarded to S.P.C. and OCE-0350834 and -0623508 awarded to J.H.C.).

References

Ahlborn, B., Harper, D. G., Blake, R. W., Ahlborn, D. and Cam, M. (1991). Fish without footprints. *J. Theor. Biol.* **148**, 521-533.

Ahlborn, B., Chapman, S., Stafford, R. and Harper, R. (1997). Experimental simulation of the thrust phases of fast-start swimming of fish. *J. Exp. Biol.* **200**, 2301-2312.

Anderson, P. A. and Schwab, W. E. (1981). The organization and structure of nerve and muscle in the jellyfish *Cyanea capillata* (Coelenterata, Scyphozoa). *J. Morphol.* **170**, 383-399.

Bone, Q. and Trueman, E. R. (1982). Jet propulsion of the calycophoran siphonophores *Chelophyes* and *Abylopsis*. *J. Mar. Biol. Assoc. U. K.* **62**, 263-276.

Bonner, J. T. (1965). *Size and Cycle*. Princeton: Princeton University Press.

Chapman, D. M. (1974). Cnidarian histology. In *Coelenterate Biology* (ed. L. Muscatine and H. M. Lenhoff), pp. 1-92. New York: Academic Press.

Costello, J. H. and Colin, S. P. (1994). Morphology and fluid motion and predation by the scyphomedusa *Aurelia aurita*. *Mar. Biol*. **121**, 327-334.

Dabiri, J. O., Colin, S. P., Costello, J. H. and Gharib, M. (2005). Flow patterns generated by oblate medusan jellyfish: field measurements and laboratory analyses. *J. Exp. Biol.* **208**, 1257-1265.

Dabiri, J. O., Colin, S. P. and Costello, J. H. (2006). Fast-swimming hydromedusae exploit velar kinematics to form an optimal vortex wake. *J. Exp. Biol.* **209**, 2025-2033.

Daniel, T. L. (1983). Mechanics and energetics of medusan jet propulsion. *Can. J. Zool.* **61**, 1406-1420.

Daniel, T. L. (1985). Cost of locomotion: unsteady medusan swimming. *J. Exp. Biol.* **119**, 149-164.

Daniel, T. L. (1995). Invertebrate swimming: integrating internal and external mechanics. *Symp. Soc. Exp. Biol.* **49**, 61-89.

DeMont, M. E. and Gosline, J. M. (1988a). Mechanics of jet propulsion in the hydromedusan jellyfish, *Polyorchis penicillatu*s. I. Mechanical properties of the locomotor structure. *J. Exp. Biol.* **134**, 313-332.

DeMont, M. E. and Gosline, J. M. (1988b). Mechanics of jet propulsion in the hydromedusan jellyfish, *Polyorchis penicillatu*s. II. Energetics of the jet cycle. *J. Exp. Biol.* **134**, 333-345.

DeMont, M. E. and Gosline, J. M. (1988c). Mechanics of jet propulsion in the hydromedusan jellyfish, *Polyorchis penicillatu*s. III. A natural resonating bell; the presence and importance of a resonant phenomenon in the locomotor structure. *J. Exp. Biol.* **134**, 347-361.

Didden, N. (1979). On the formation of vortex rings: rolling-up and production of circulation. *Z. Angew. Math. Phys.* **30**, 101-116.

Donaldson, S., Mackie, G. O. and Roberts, A. (1980). Preliminary observations on escape swimming and giant neurons in *Aglantha digitale* (Hydromedusae: Trachylina). *Can. J. Zool.* **58**, 549-552.

Fawcett, D. W. (1994). *A Textbook of Histology*. New York: Chapman & Hall.

Ford, M. D. and Costello, J. H. (2000). Kinematic comparison of bell contraction by four species of hydromedusae. *Sci. Mar*. **64**, 47-53.

Gladfelter, W. B. (1972a). Structure and function of the locomotory system of *Polyorchis montereyensis* (Cnidaria, Hydrozoa). *Helgolander Wiss. Meeresunters* **23**, 38-79.

Gladfelter, W. B. (1972b). Structure and function of the locomotory system of scyphomedusa *Cyanea capillata*. *Mar. Biol.* **14**, 150-160.

Kramp, P. L. (1959). The Hydromedusae of the Atlantic Ocean and adjacent waters. *Dana Rep.* **46**, 1-283.

Kramp, P. L. (1961). Synopsis of the medusae of the world. *J. Mar. Biol. Assoc. U. K.* **40**, 1-469.

Kramp, P. L. (1968). The hydromedusae of the Pacific and Indian Oceans. *Dana Rep.* **72**, 1-200.

Lighthill, M. J. (1960). Note on the swimming of slender fish. *J. Fluid Mech.* **9**, 305-317.

Mackie, G. O. (1980). Slow swimming and cyclical 'fishing' behavior in *Aglantha digitale* (Hydromedusae: Trachylina). *Can. J. Fish. Aquat. Sci.* **37**, 1550-1556.

Mayer, A. G. (1910). Medusae of the World. Vol. 1 and 2, the Hydromedusae. Vol. 3, the Scyphomedusae. *Carnegie Inst. Washington Publ.* **109**, 1-735.

Omori, M. and Kitamura, M. (2004). Taxonomic review of three Japanese species of edible jellyfish (Scyphozoa: Rhizostomeae). *Plankton Biol. Ecol.* **51**, 36-51.

Pugh, P. R. (1999). Siphonophorae. In *South Atlantic Zooplankton* (ed. D. Boltovskoy), pp. 467-511. The Netherlands: Backhuys Publishers.

Saffman, P. G. (1992). *Vortex Dynamics*. Cambridge: Cambridge University Press.

Thompson, D. W. (1961). *On Growth and Form*. Cambridge: Cambridge University Press.

Valentine, J. W. (2004). *On the Origin of Phyla*. Chicago: Chicago University Press.

Vogel, S. (2003). *Comparative Biomechanics*. Princeton: Princeton University Press.